

Topological two-particle dynamics in a periodically driven lattice model with on-site interactions

Anna Berti and Iacopo Carusotto

INO-CNR BEC Center and Dipartimento di Fisica, Università di Trento, 38123 Trento, Italy

(Dated: September 14, 2021)

We develop a realistic protocol to observe a robust topological dynamics of two-particle bound states in a lattice model with on-site interactions and suitably designed time-dependent hoppings. This Floquet scheme can be realistically implemented on existing digital quantum computer platforms. Marked differences from the topological single-particle dynamics of two independent particles and clear signatures of the entanglement between the two constituent particles are highlighted.

Since their discovery, quantum Hall effects in two-dimensional electron gases under strong magnetic fields have been the subject of many theoretical and experimental studies highlighting their strong connection with topology concepts [1–8]. Besides electronic materials, the topological single-particle dynamics underlying the integer quantum Hall effect has been experimentally investigated in several other systems, including cold atomic gases [9] and photonic platforms [10–12]. In the presence of interactions, a much richer physics is found in the strongly correlated states underlying the fractional quantum Hall effect, including fractional charge and statistics of anyonic excitations [13] and exciting perspectives in the direction of topological quantum computing [14]. First steps in this direction have been recently reported using cold atomic gases in optical lattices [15, 16], Rydberg atoms [17] and polaritons [18], and superconductor-based circuit-QED systems [19–21].

With the recent progress on digital quantum computing (QC) devices, platforms hosting a lattice of qubits and allowing for discrete single- and two-qubit gate operations between neighboring sites [22–24] appear as promising platforms to explore many-body phenomena. In these QC platforms, the discrete unitary operations are applied in a sequence, so to guarantee that each site is subject to a single operation during each time-step. While this is usually a necessary step in the optimization of a QC device, it is responsible for the typical complications of time-dependent Hamiltonians, typically chosen with a time-periodic Floquet form. In a good trotterization limit where many small steps are performed at a fast rate, the ordering of operations becomes irrelevant and the Floquet evolution approximately recovers a static model. However, since in any realistic device only a limited number of operations can be performed before losing coherence it is beneficial to adopt sizable unitary operations, so that the temporal modulation can have a substantial impact on the dynamics [25–27].

As an illustration of the potential and the complexities of this Floquet approach, this Letter reports a detailed investigation of the topological dynamics of two-particle bound states, the so-called doublons [28–31]. In spite of energy being conserved only modulo the Floquet energy,

suitable working points are found where doublon states can not dissociate into free particles and a clean unidirectional propagation of doublons around the system edge is anticipated. In its simplicity, such a two-body effect is an example of a subtle interplay between topology and interactions and is a preliminary step towards the realization of topological many-body states of photonic matter [32].

The model – We consider a two-dimensional bosonic lattice system of Hamiltonian

$$\mathcal{H}(t) = - \sum_{ij} \left(J_{ij}(t) a_i^\dagger a_j + \text{h.c.} \right) + \frac{U}{2} \sum_i a_i^\dagger a_i^\dagger a_i a_i \quad (1)$$

where a_i^\dagger (a_i) is the creation (annihilation) operator for a particle in the i -th site. Interactions are assumed to be on-site with strength U and are active at all time, as implemented in superconducting QC platforms [20].

With an eye to digital QC frameworks [22], the hopping coefficients $J_{ij}(t)$ are instead taken time-periodic of period T . We assume that each period is split in a sequence of N sub-periods of equal duration $\tau = T/N$. During each sub-period $[(n-1)\tau, n\tau]$ (with $n = 1, \dots, N$) the time-independent hamiltonian $\mathcal{H}(t) = \mathcal{H}_n$ features a constant hopping strength between a given set of pairs of neighboring sites $\langle ij \rangle_n$ with non-trivial hopping phases, $J_{ij}(t) = J_{ij}^n = J e^{i\phi_{ij}^n}$. An example of such configuration is illustrated in Fig.1. During each sub-interval, only the links of the corresponding color are active (left panel). The order of activation is indicated in the right panel. Both interactions and complex hoppings can be implemented on existing QC platforms, respectively by exploiting non-linear effects [33] and engineering artificial gauge fields [34–37].

Single-particle physics – We start our investigation by looking at the topological properties of the single-particle bands arising from our Hamiltonian (1). Given its discrete temporal periodicity, within the Floquet theory [25–27] the single particle bands arise as the eigenvalues of the Floquet operator, namely the time-evolution operator along a period T . Since during each sub-interval the Hamiltonian is time-independent, the Floquet operator $\mathcal{U}(T)$ can be written as the product of the N unitary operators associated to each hopping step, $\mathcal{U}(T) = \prod_{n=1}^N e^{-i\mathcal{H}_n\tau}$. Since the pairs $\langle ij \rangle_n$ of sites

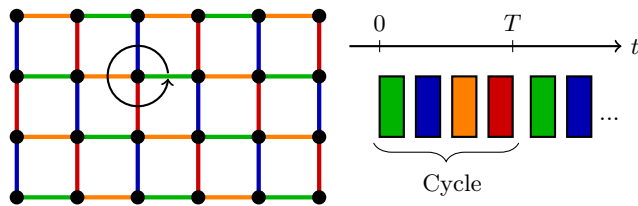


FIG. 1. Scheme of the two-dimensional square lattice under investigation. Each color identifies the hopping links that are active during each time-interval according to the temporal sequence shown on the right. The arrow indicates the chirality of the hopping scheme.

involved in each step are disconnected, the exponential $e^{-i\mathcal{H}_n\tau}$ can be expanded as a block matrix in the single particle basis. The block corresponding to each pair ij is a hopping matrix with hopping angle $\theta = J\tau$,

$$U_H(\theta, \phi) = e^{iJ\tau(\hat{u}\cdot\vec{\sigma})} = \begin{pmatrix} \cos\theta & i\sin\theta e^{i\phi} \\ i\sin\theta e^{-i\phi} & \cos\theta \end{pmatrix} \quad (2)$$

while the sites not involved in any pair are left intact.

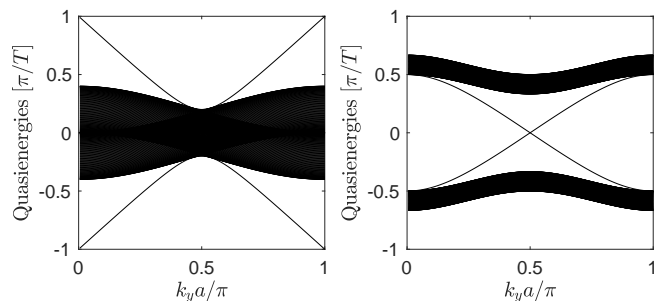


FIG. 2. Single-particle Floquet quasi-energy bands for an anomalous Floquet insulator (AFI) model with $\theta = 0.6\pi$ (left panel) and for a Harper-Hofstadter-Floquet (HHF) model with $\alpha = 1/2$ and $\theta = \pi/4$ (right panel). Both spectra are computed for a cylindrical geometry with 100 sites along x .

In the good trotterization limit $\theta \ll 1$, the full Floquet operator $\mathcal{U}(T)$ can be accurately approximated by the exponential of a static Hamiltonian; hence the condition $\theta \ll 1$ allows the realization of most standard time-independent topological models. In this work we go beyond this regime and we look for features that stem from the Floquet character of our dynamics. As we are going to see, the topology of the single-particle bands of this Floquet tight-binding model is not only determined by the values of θ and ϕ_{ij}^n , but may also depend on the hopping sequence. Two most remarkable examples of this physics are illustrated in Fig.2.

In the left panel, we consider the anomalous Floquet insulator (AFI) model of [27], which is naturally realized using the hopping sequence described in Fig.1 with trivial hopping phases $\phi_{ij}^n = 0$ for all i, j, n . For a finite system in the form of a strip with periodic boundary conditions

along y and a finite size along x , the spectrum involves a single bulk band plus a pair of dispersive edge states on each side that span across the whole quasienergy Brillouin zone.

In the right panel we consider a Harper-Hofstadter-Floquet (HHF) model with magnetic flux $\alpha = 1/2$. In our calculation, a synthetic vector gauge potential along y is realized by imposing $\phi_{ij}^n = \pi x_i$ for all links directed along the positive- y direction. In contrast to the non-topological nature of the time-independent HH model at $\alpha = 1/2$ with the two bands touching at a Dirac point, the chirality of the Hopping sequence considered in our calculations as indicated in Fig.1 leads to the opening of a finite topological gap. This is witnessed by the appearance of topological edge states within the gap and by the onset of finite (and opposite) values of the Chern numbers of the two bands. Of course, the width of the topological gap is only sizable for sizable values of the hopping phase θ (here we have used $\theta = \pi/4$), and closes down as one approaches the trotterized limit $\theta \rightarrow 0$ recovering the time-independent limit. These single-particle bands are the starting point of our analysis of two-particle bound states, the so-called doublons.

Two-particle bound states – In the time-independent case, the energy of a doublon is typically of the order of the interaction strength U whereas the continuum of scattering states is characterized by a bandwidth of the order of the hopping coefficients J_{ij} . In the strongly interacting limit $|U| \gg |J_{ij}|$, doublons are thus isolated states in the two-particle spectrum and processes in which a doublon decays into its constituents are forbidden by energy conservation [28–31]: the energy that would be released in such a decay processes is too high to be absorbed by the kinetic energy of the products. As a result, doublons are metastable states which can only decay via more complex multi-particle processes.

In this regime, perturbation theory in $J_{ij}/|U|$ can be used to understand the topological properties of the energy bands of two-body states by deriving an effective single particle Hamiltonian for doublons in the usual form,

$$\mathcal{H}_{\text{eff}} = U \sum_i \alpha_i^\dagger \alpha_i - \sum_{ij} \left(J_{ij}^{\text{eff}} \alpha_i^\dagger \alpha_j + \text{h.c.} \right) \quad (3)$$

where $\alpha_i = a_i a_i / \sqrt{2}$ is the destruction operator for a doublon on the i site. The effective hopping coefficients J_{ij}^{eff} for doublons can be extracted from the ones of the underlying single-particle model by identifying the sequential single-particle hopping processes leading to an overall two-particle hopping. Such an approach has been used in studies of the band topology of doublons in different lattice geometries for time-independent Hamiltonians [38–42].

For periodically driven systems, we can still define a doublon as a localized state of two particles but the strong interaction assumption is no longer sufficient to

guarantee the stability of doublon states. Since the spectrum of Floquet systems is periodic by $\Omega = 2\pi/T$ along the energy direction, one must in fact ensure that the band of doublon states never overlaps with any Floquet replica of the single-particle states. A sufficient condition is of course to work in the trotterized limit of a very fast Floquet frequency $\Omega \gg |U| \gg |J_{ij}|$ where the Floquet problem can be accurately reformulated in terms of an effective time-independent Hamiltonian.

From a practical point of view, this regime is however not a favourable one in view of implementations on a digital quantum computer device as it requires a large number $\sim \Omega/|J_{ij}|$ of elementary operations to be performed during the characteristic time of the particle motion, with the consequent loss of coherence growth of errors. It is therefore of great interest to devise configurations where the doublons are stable in regimes where the three energy scales Ω , U , J_{ij} are comparable.

Our proposed procedure starts from the computation of the time-evolution operator during a single step of the Floquet evolution in the basis of two-particle states. Consider a generic site i and the time-interval n in which it is coupled to the neighboring site j . The three two-particle states coupled by the Hamiltonian \mathcal{H}_n are indicated as $|ii\rangle$, $|ij\rangle$ and $|jj\rangle$: the first and the third states are doublons localized at the i, j sites respectively; the second state contains a particle in each site. In this basis, exponentiation of \mathcal{H}_n gives the time evolution operator

$$U = e^{-i\gamma/2} \begin{pmatrix} U_{11} & U_{12}e^{i\phi} & U_{13}e^{2i\phi} \\ U_{12}e^{-i\phi} & U_{22} & U_{12}e^{i\phi} \\ U_{13}e^{-2i\phi} & U_{12}e^{-i\phi} & U_{11} \end{pmatrix} \quad (4)$$

whose matrix elements involve the coefficients

$$U_{11} = \frac{1}{2} \left[e^{-i\gamma/2} + \cos(\gamma'/2) - i\frac{\gamma}{\gamma'} \sin(\gamma'/2) \right] \quad (5)$$

$$U_{12} = i\frac{2\sqrt{2}\theta}{\gamma'} \sin(\gamma'/2) \quad (6)$$

$$U_{13} = \frac{1}{2} \left[-e^{-i\gamma/2} + \cos(\gamma'/2) - i\frac{\gamma}{\gamma'} \sin(\gamma'/2) \right] \quad (7)$$

$$U_{22} = \cos(\gamma'/2) + i\frac{\gamma}{\gamma'} \sin(\gamma'/2) \quad (8)$$

defined in terms of $\gamma = U\tau$ and $\gamma' = \sqrt{\gamma^2 + 16\theta^2}$.

In order to obtain a closed dynamics within the space of doublon states, we need to initialize the system in a doublon state and then prevent doublons from dissociating into single-occupancy states during the whole evolution. In terms of the time-evolution matrix (4), this requires that $U_{12} = 0$, which in turn imposes:

$$\left(\frac{U}{J}\right)^2 = \frac{4k^2}{(\theta/\pi)^2} - 16 \quad (9)$$

for some integer k for which the RHS is positive.

Under the condition (9), the second row and column of the time evolution matrix decouples from the two other and we can recast (4) in terms of a two-by-two hopping matrix for doublon states in the i, j sites analogous to (2) with effective hopping angle θ' and phase shift ϕ'

$$\theta' = \frac{\pi}{2} \left(\text{mod}(k, 2) \pm \sqrt{k^2 - (2\theta/\pi)^2} \right) \text{ and } \phi' = 2\phi. \quad (10)$$

Summarizing, equation (9) gives the specific values of U/J for which the two-particle dynamics can be reduced to an effective one-body dynamics for doublons with the effective parameters θ', ϕ' in (10). From these, it is then straightforward to establish whether the energy bands have non-trivial topological properties.

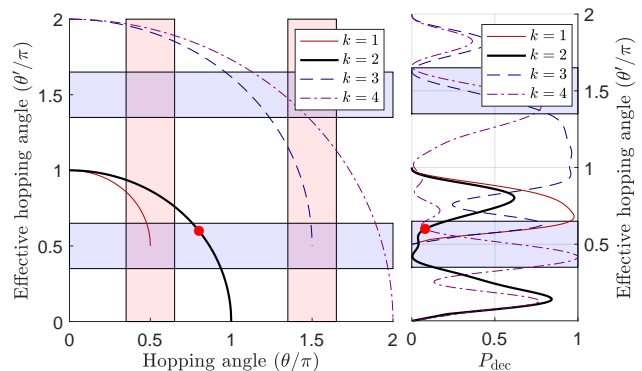


FIG. 3. Left panel: functions $\theta'(\theta)$ given by (10) and defining the stability of doublon states, for different values of k and $U > 0$. Red (blue) areas indicate a non-trivial band topology for single-particle (doublons) for trivial hopping phases $\phi_{ij} = \phi'_{ij} = 0$; they are estimated by looking for the presence of edge states. Right panel: probability that two doublons occupying coupled neighbouring sites remain intact at the end of a hopping step as a function of θ' for different k and assuming $U > 0$. The red dots indicate the parameter values adopted in the following Figures.

The curves in Fig.3 show the function $\theta'(\theta)$ given by (10) for $k = 1, 2, 3, 4$. The red and blue shadings respectively indicate the parameter ranges for which the one-body and two-body dynamics are topological in the case of trivial hopping phases $\phi = \phi' = 0$ for all pairs of sites. Quite interestingly, this plot shows that the doublon band may display non-trivial topological properties in spite of the underlying single-particle model being topologically trivial.

In the strongly interacting limit $|U| \gg |J|$, the decoupling condition (9) can be satisfied with $k \gg 1$ and the effective hopping angle for doublons is (modulo π) $\theta' \sim -2J\theta/|U| = (-2J^2/|U|)\tau$. This corresponds to an effective hopping coefficient $J_{\text{eff}} = 2J^2/|U|$ equal to the one that one would get for a static system using perturbation theory. This conclusion holds under no assumption on the value of θ and proves that, independently of the presence or absence of the periodic driving, the dynamics

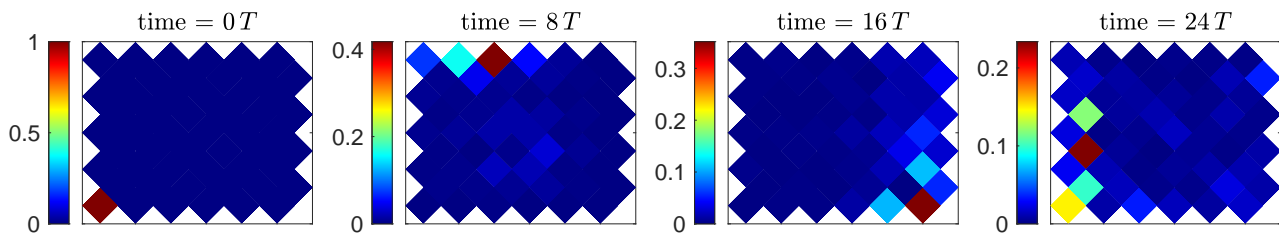


FIG. 4. Numerical simulation of the time-evolution on a $N_{\text{sites}} = 54$ sites lattice. For each site, the color indicates the probability of having a doublon at that position, $A_l = |\langle \psi | ll \rangle|^2$. System parameters: $\phi_{ij} = 0$, $\theta = 0.8\pi$, $U = 3J$ as indicated by the red dot in Fig.3. The system is initialized with a doublon on the bottom-left corner. The doublon then evolves in the clock-wise direction around the system.

of doublons is always very slow in the strongly interacting limit, $|\theta'| \ll \theta$. Once again, this is not a convenient regime for an experiment, since it requires a large number of gate operation at the cost of introducing significant errors. As a consequence, all the calculations that follow will focus on the smallest values of U that are solutions of the decoupling condition (9).

Doublon dynamics – In order to highlight the main features of the topological two-particle dynamics, we focus our attention on a configuration with $\phi = \phi' = 0$, $\theta = 0.8\pi$ and $U = 3J$. This parameter choice (indicated by the red dot in Fig.3) satisfies (9) with $k = 2$ and gives a sizable value of the effective hopping angle $\theta' = 0.6\pi$ for which the two-body evolution is topological (as shown in the one-body spectrum in the left panel of Fig. 2). The time-evolution starting from a doublon state is reported in Fig.4: as expected, the spatial distribution of the double-occupancies $A_l = |\langle \psi | ll \rangle|^2$ unidirectionally circulates around the edge while spreading in space because of the non-zero group velocity dispersion of the doublon edge state. As typical for a chiral dynamics, the wavepacket is able to turn around corners without suffering any backscattering.

Further light on the two-particle nature of this topological dynamics is obtained by comparing the evolution reported in figure 4 with the one of a non-interacting HHF model at flux $\alpha = 1/2$ with a hopping angle $\theta = \pi/4$ for which the two particles evolve independently from each other and the topology is present at the single-particle level (right panel of figure 2). While A_l has a similar evolution in the two cases, crucial differences are visible in the left panel of Fig.5. For the topological doublons, the condition (9) guarantees that the overlap $\mathcal{O}_d = \sum_l A_l$ with the subspace of doublon states remains perfect during the evolution (solid red line) and still suffers minor losses at the end of a round trip if this condition is only approximately satisfied (dashed red line). On the other hand, in the single-particle topology case, \mathcal{O}_d has already significantly dropped after a few Trotter steps (black line): since there is nothing that can keep the two particles together, their relative wavefunction is free to spread under the effect of the edge state dispersion.

Additional microscopic details of this doublon dynamics are visible in the middle and right panels of Fig.5. Here, the components of the two-body wavefunction at time $t = 24T$ on the basis of two-particle states $|l_1 l_2\rangle$ are plotted for the same two cases. For non-interacting particles, the wavefunction of the system is the tensor product of the two single-particle states. This is illustrated by the checkerboard pattern visible in the right panel of Fig.5. In the case of topological doublons, instead, the wavefunction consists of a superposition of doublon states at different positions and keeps displaying a strong entanglement between the two particles: as it is visible in the middle panel of Fig.5, a measurement of the position of the first particle provides full information on the other particle's position. When written in the computational basis of the quantum computer device, the state with a delocalized doublon along the edge can be seen as a generalized W state for a system of N_{sites} qutrits. As such, it can be straightforwardly revealed in a QC platform.

Towards a many-body dynamics – In order to assess the promise of our scheme as a building block for a full-fledged many-doublon physics, we need to check the stability of a pair of doublons located on neighboring sites. As long as the two sites are not coupled, the two doublons do not affect each other and maintain their stability. During the time intervals where the two sites are coupled, undesired processes where the doublons exchange particles and decay into a three body complex plus a free particle or merge into a single four-body complex may occur. Assuming for simplicity a two-body form of interactions as included in (1), the interaction energy quickly grows with the number of excitations present. This suggests that the three- and four-body complexes are strongly detuned and their occupation remains small in spite of the interval τ being relatively short and allowing for sizable departures from energy conservation. This guess is quantitatively validated in the right panel of Fig.3 where we show the probability P_{dec} for a pair of neighboring doublons to be decayed at the end of the hopping step for parameters exactly satisfying (9) for different k 's. In a sizable window of parameter space including our operating point, this probability remains below 10%. As it is shown in

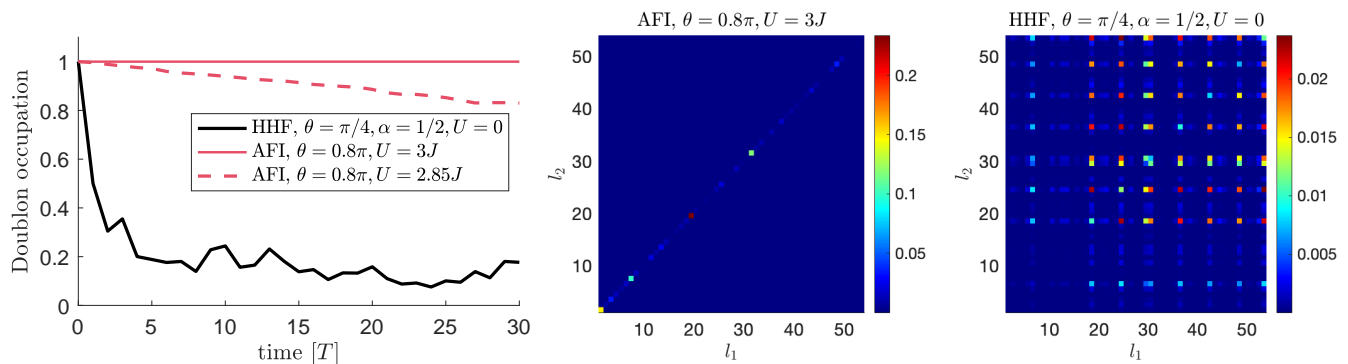


FIG. 5. Left panel: time evolution of the overlap of the wavefunction with the doublon subspace for the AFI model with two different choices of parameters, exactly satisfying the stability condition (9) (solid red) and slightly departing from it by 5% (red dashed). For comparison, the black line shows the same quantity for a non-interacting HHF model with single-particle topology only. Middle and right panels: squared modulus $|\langle \psi | l_1 l_2 \rangle|^2$ of the wavefunction, at time $t = 24T$, in the (l_1, l_2) basis labelled by the position of the two particles. Here, the doublon states correspond to the main diagonal. The middle (right) panels are for the interacting AFI (non-interacting HHF) models. Same system geometry of Fig.4.

the Supplemental Material, a further reduced P_{dec} can be obtained by including additional interaction terms in the model. This confirms the potential of our system for studies of many-doublon physics.

Conclusions – In this work we have proposed a realistic protocol to observe a topological Floquet dynamics for two-particle bound states in a lattice model with time-dependent hoppings and on-site interactions. Conditions for the stability of doublons are formulated, which appear promising in view of scaling up the framework towards many-body states. Our results suggest the potential of digital quantum computer platforms for studies of novel phases of synthetic photonic matter in a Floquet context.

Acknowledgements – We are grateful to Z. Cian, M. Hafezi, E. Kapit, Z. Jiang, E. Jones, C. Neill, P. Roushan for continuous stimulating exchanges. We acknowledge financial support from the Provincia Autonoma di Trento, the Q@TN initiative, the European Union FET-Open grant “MIR-BOSE” (n.737017), from the H2020-FETFLAG-2018-2020 project “PhoQuS” (n.820392) and from Google via the quantum NISQ award.

[1] K. v. Klitzing, G. Dorda, and M. Pepper, *Phys. Rev. Lett.* **45**, 494 (1980).
 [2] D. C. Tsui, H. L. Stormer, and A. C. Gossard, *Phys. Rev. Lett.* **48**, 1559 (1982).
 [3] D. Tong, Lectures on the quantum hall effect, arXiv preprint arXiv:1606.06687 (2016).
 [4] D. J. Thouless, M. Kohmoto, M. P. Nightingale, and M. den Nijs, *Phys. Rev. Lett.* **49**, 405 (1982).
 [5] R. B. Laughlin, *Phys. Rev. Lett.* **50**, 1395 (1983).
 [6] D. Arovas, J. R. Schrieffer, and F. Wilczek, *Phys. Rev. Lett.* **53**, 722 (1984).
 [7] B. A. Bernevig, *Topological Insulators and Topological Superconductors* (Princeton University Press, 2013).

[8] M. Franz and L. Molenkamp, *Topological Insulators*, ISSN (Elsevier Science, 2013).
 [9] N. R. Cooper, J. Dalibard, and I. B. Spielman, *Rev. Mod. Phys.* **91**, 015005 (2019).
 [10] F. D. M. Haldane and S. Raghu, *Phys. Rev. Lett.* **100**, 013904 (2008).
 [11] Z. Wang, Y. Chong, J. D. Joannopoulos, and M. Soljačić, *Nature* **461**, 772 (2009).
 [12] T. Ozawa, H. M. Price, A. Amo, N. Goldman, M. Hafezi, L. Lu, M. C. Rechtsman, D. Schuster, J. Simon, O. Zilberberg, and I. Carusotto, *Topological photonics*, *Rev. Mod. Phys.* **91**, 015006 (2019).
 [13] A. Stern, Fractional topological insulators - a pedagogical review, *Annual Review of Condensed Matter Physics* **7** (2015).
 [14] C. Nayak, S. H. Simon, A. Stern, M. Freedman, and S. Das Sarma, *Rev. Mod. Phys.* **80**, 1083 (2008).
 [15] P. M. Preiss, R. Ma, M. E. Tai, A. Lukin, M. Rispoli, P. Zupancic, Y. Lahini, R. Islam, and M. Greiner, *Strongly correlated quantum walks in optical lattices*, *Science* **347**, 1229–1233 (2015).
 [16] M. E. Tai, A. Lukin, M. Rispoli, R. Schittko, T. Menke, D. Borgnia, P. M. Preiss, F. Grusdt, A. M. Kaufman, and M. Greiner, *Nature* **546**, 519–523 (2017).
 [17] S. de Léséleuc, V. Lienhard, P. Scholl, D. Barredo, S. Weber, N. Lang, H. P. Büchler, T. Lahaye, and A. Browaeys, *Science* **365**, 775 (2019).
 [18] L. W. Clark, N. Schine, C. Baum, N. Jia, and J. Simon, *Nature* **582**, 41 (2020).
 [19] P. Roushan, C. Neill, A. Megrant, Y. Chen, R. Babush, R. Barends, B. Campbell, Z. Chen, B. Chiaro, A. Dunsworth, *et al.*, *Nature Physics* **13**, 146–151 (2016).
 [20] Y. Ye *et al.*, *Phys. Rev. Lett.* **123**, 050502 (2019).
 [21] A. Blais, A. L. Grimsmo, S. M. Girvin, and A. Wallraff, *Circuit quantum electrodynamics*, *Rev. Mod. Phys.* **93**, 025005 (2021).
 [22] F. Arute *et al.*, *Nature* **574**, 505–510 (2019).
 [23] M. Nielsen and I. Chuang, *Quantum Computation and Quantum Information: 10th Anniversary Edition* (Cambridge University Press, 2010).

- [24] L. Gyongyosi and S. Imre, *Computer Science Review* **31**, 51 (2019).
- [25] M. Holthaus, *Journal of Physics B: Atomic, Molecular and Optical Physics* **49**, 013001 (2015).
- [26] N. Goldman and J. Dalibard, *Physical review X* **4**, 031027 (2014).
- [27] M. S. Rudner, N. H. Lindner, E. Berg, and M. Levin, *Phys. Rev. X* **3**, 031005 (2013).
- [28] K. Winkler, G. Thalhammer, F. Lang, R. Grimm, J. Hecker Denschlag, A. J. Daley, A. Kantian, H. P. Büchler, and P. Zoller, *Nature* **441**, 853–856 (2006).
- [29] D. Petrosyan, B. Schmidt, J. R. Anglin, and M. Fleischhauer, Quantum liquid of repulsively bound pairs of particles in a lattice, *Physical Review A* **76**, 033606 (2007).
- [30] M. Valiente and D. Petrosyan, *Journal of Physics B: Atomic, Molecular and Optical Physics* **41**, 161002 (2008).
- [31] S. Fölling, S. Trotzky, P. Cheinet, M. Feld, R. Saers, A. Widera, T. Müller, and I. Bloch, Direct observation of second-order atom tunnelling, *Nature* **448**, 1029 (2007).
- [32] I. Carusotto, A. A. Houck, A. J. Kollár, P. Roushan, D. I. Schuster, and J. Simon, *Nature Physics* **16**, 268 (2020).
- [33] D. Roy, C. M. Wilson, and O. Firstenberg, *Rev. Mod. Phys.* **89**, 021001 (2017).
- [34] M. Aidelsburger, S. Nascimbene, and N. Goldman, *Comptes Rendus Physique* **19**, 394 (2018).
- [35] J. Dalibard, F. Gerbier, G. Juzeliūnas, and P. Öhberg, Colloquium: Artificial gauge potentials for neutral atoms, *Rev. Mod. Phys.* **83**, 1523 (2011).
- [36] M. Aidelsburger, M. Atala, S. Nascimbène, S. Trotzky, Y.-A. Chen, and I. Bloch, *Phys. Rev. Lett.* **107**, 255301 (2011).
- [37] N. Goldman, G. Juzeliūnas, P. Öhberg, and I. B. Spielman, *Reports on Progress in Physics* **77**, 126401 (2014).
- [38] M. A. Gorlach and A. N. Poddubny, *Phys. Rev. A* **95**, 053866 (2017).
- [39] M. Di Liberto, A. Recati, I. Carusotto, and C. Menotti, *Phys. Rev. A* **94**, 062704 (2016).
- [40] G. Salerno, M. Di Liberto, C. Menotti, and I. Carusotto, *Phys. Rev. A* **97**, 013637 (2018).
- [41] G. Salerno, G. Palumbo, N. Goldman, and M. Di Liberto, *Phys. Rev. Research* **2**, 013348 (2020).
- [42] P. M. Azcona and C. A. Downing, *Scientific Reports* **11**, 10.1038/s41598-021-91778-z (2021).
- [43] M. Hafezi, A. S. Sørensen, E. Demler, and M. D. Lukin, *Phys. Rev. A* **76**, 023613 (2007).

Supplemental material – In order to assess the robustness of doublons, we compute here the probability that a pair of doublons occupying neighbouring sites merge or exchange particles during a hopping step connecting the two sites. Let us focus on a pair of sites and let us call a, b (a^\dagger, b^\dagger) the annihilation (creation) operators for single particles on those sites. Including three- and four-body interactions of strength respectively U' and U'' , the Hamiltonian reads:

$$\mathcal{H} = -J(a^\dagger b + b^\dagger a) + \frac{U}{2} \sum_{x=a,b} (x^\dagger)^2 (x)^2 + \sum_{x=a,b} \left[\frac{U'}{3!} (x^\dagger)^3 (x)^3 + \frac{U''}{4!} (x^\dagger)^4 (x)^4 \right] \quad (11)$$

In our case of four particles distributed among two sites, we can use the following basis of five orthonormal states:

$$\begin{aligned} |D\rangle &= \frac{1}{2} a^\dagger a^\dagger b^\dagger b^\dagger |\text{vac}\rangle \equiv \alpha^\dagger \beta^\dagger |\text{vac}\rangle \\ |T_a\rangle &= \frac{1}{\sqrt{3!}} a^\dagger a^\dagger a^\dagger b^\dagger |\text{vac}\rangle & |T_b\rangle &= \frac{1}{\sqrt{3!}} a^\dagger b^\dagger b^\dagger b^\dagger |\text{vac}\rangle \\ |Q_a\rangle &= \frac{1}{\sqrt{4!}} a^\dagger a^\dagger a^\dagger a^\dagger |\text{vac}\rangle & |Q_b\rangle &= \frac{1}{\sqrt{4!}} b^\dagger b^\dagger b^\dagger b^\dagger |\text{vac}\rangle \end{aligned}$$

The first one is a pair of doublons sitting at sites a and b ; the second (third) is a triplet on site a (b) plus a single particle in site b (a); the fourth (fifth) is a four-body state on site a (b). Within this basis, the matrix representation of the hamiltonian is:

$$H = \begin{pmatrix} 2U & -\sqrt{6}J & -\sqrt{6}J & 0 & 0 \\ -\sqrt{6}J & H_T & 0 & -2J & 0 \\ -\sqrt{6}J & 0 & H_T & 0 & -2J \\ 0 & -2J & 0 & H_Q & 0 \\ 0 & 0 & -2J & 0 & H_Q \end{pmatrix}$$

where $H_T = U' + 3U$ and $H_Q = U'' + 4U' + 6U$ are the interaction energies of a three- and four-body state respectively. If we call $M = \exp(-iH\tau)$ the time evolution operator after a trotter step, the probability that the doublons do not remain intact is:

$$P_{\text{dec}} = 1 - |M_{11}|^2 \quad (12)$$

The left panel of Fig. 3 in the main text shows the trend of P_{dec} as a function of the effective hopping angle θ' when $U' = U'' = 0$ and U is a solution of the decoupling condition Eq.(9) for $k = 1, 2, 3, 4$: there exists a sizeable window of values of θ' , close to $\pi/2$, for which the two-body evolution is both topological and robust under doublon decay, because $P_{\text{dec}} \ll 1$. In particular, at our working point (the red dot in Fig. 3), we find $P_{\text{dec}} \simeq 8\%$ while an optimal value around $P_{\text{dec}} \sim 0.4\%$ can be obtained with a better tuned $\theta' \simeq 0.42\pi$.

If needed, the stability of doublons can be further improved by considering three- and four-body interactions.

The simplest strategy consists in setting $U' \gg J$: we expect such condition to bring triplets and quadruplets out of resonance, leading to a decay probability P_{dec} closer to 0 for all hopping angles and for any value of U'' . Indeed, once three-body interactions are sufficiently strong, both H_T and H_Q are already much larger than J , without the need of including four-body terms in the hamiltonian. The left panel of Fig. 6 shows the decay probabilities obtained with $U' = 10J$ and $U'' = 0$: the curves remain below 30% for all hopping angles. At our working point, identified again by the red dot, we obtain $P_{\text{dec}} \simeq 4\%$. Better results are found when further increasing U'/J . We verified that adding four-body interactions (we tried in the range $[0, 10^6]$) does not modify significantly the decay probabilities.

Along the same lines of what we did in the main text for single doublon hopping, we can avoid the strongly interacting regime and proceed to a fine-tuning of U', U'' in order to minimize P_{dec} for all hopping angles. A rigorous procedure to find the optimal values of $U'(\theta), U''(\theta)$ would require the exact analytical computation of the matrix M and the minimization of the coefficients M_{1l} , $l \neq 1$. Here we restrict ourselves to showing that, once the working point is fixed, one can properly tune U' and U'' in order to minimize P_{dec} . This procedure is illustrated in the right panel of Fig. 6 where, for instance, we obtained a decay probability as low as $P_{\text{dec}}(\theta' = 0.6\pi) = 0.02\%$ by tuning $U' = 0.45J$ and $U'' = J$.

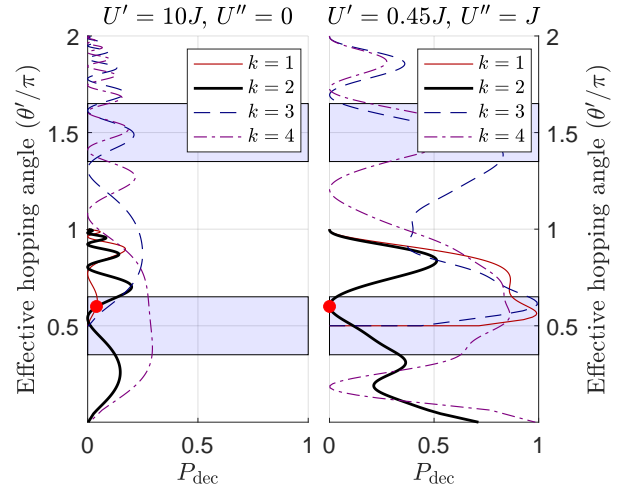


FIG. 6. Doublon decay probabilities as a function of the effective hopping angle with U satisfying the the decoupling condition Eq.(9) for $k = 1, 2, 3, 4$. Blue shaded areas are topological for the doublon dynamics. The red dot indicates the working point of Fig.4 with $\theta' = 0.6\pi$ and $U = 3J$. Left panel: strongly interacting regime, $U' = 10J$, $U'' = 0$. Right panel: fine tuning procedure with $U' = 0.45J$ and $U'' = J$.